

Charge transfer in spinel Co_3O_4 at high pressures

This article has been downloaded from IOPscience. Please scroll down to see the full text article.

2012 J. Phys.: Condens. Matter 24 435401

(<http://iopscience.iop.org/0953-8984/24/43/435401>)

View [the table of contents for this issue](#), or go to the [journal homepage](#) for more

Download details:

IP Address: 164.54.164.8

The article was downloaded on 08/10/2012 at 14:42

Please note that [terms and conditions apply](#).

Charge transfer in spinel Co_3O_4 at high pressures

Ligang Bai¹, Michael Pravica¹, Yusheng Zhao¹, Changyong Park², Yue Meng², Stas V Sinogeikin² and Guoyin Shen²

¹ Department of Physics and Astronomy, University of Nevada Las Vegas and High Pressure Science and Engineering Center (HiPSEC), Las Vegas, NV 89154-4002, USA

² High Pressure Collaborative Access Team, Geophysical Laboratory, Carnegie Institution of Washington, Argonne, IL 60439, USA

E-mail: BaiLg@hpcat.aps.anl.gov

Received 25 July 2012, in final form 23 August 2012

Published 3 October 2012

Online at stacks.iop.org/JPhysCM/24/435401

Abstract

Charge transfer in cobalt oxide Co_3O_4 in the spinel structure is evidenced by experimental results using x-ray diffraction (XRD), x-ray absorption near edge structure (XANES) spectroscopy, and Raman scattering at high pressures up to 42.1, 24.6 and 35.1 GPa, respectively. While the cubic structure was found to persist under pressure up to 42.1 GPa based on the XRD and Raman results, the mode Grüneisen parameter was calculated according to our Raman measurements. Our structural data refinement revealed a structural transition from the normal spinel structure at low pressures to a partially inverse spinel structure at pressures above 17.7 GPa. This transition may be caused by the interaction of charges between tetrahedral and octahedral sites via a charge transfer process. Evidence for the charge transfer process is further supported by changes of the pre-edge features in the XANES data.

(Some figures may appear in colour only in the online journal)

1. Introduction

Spinel, either normal or inverse type, is of great interest in both basic and technological research. The normal spinel structure can be expressed as $(\text{A})[\text{B}]_2\text{O}_4$, where A and B denote the divalent and trivalent cations, and the parentheses and square brackets represent tetrahedral and octahedral sites, respectively. The inverse spinel can be expressed as $(\text{B})[\text{AB}]\text{O}_4$, with the A cation occupying one half of the octahedral coordination sites, and the B cation occupying the other half of the octahedral coordination sites as well as the tetrahedral coordination sites. In the intermediate or mixed spinels, elements A and B are distributed in both octahedral and tetrahedral sites. These spinels display many intriguing phenomena, such as order–disorder transition [1–3], insulator–metal transition [4–6], and magnetic transition [7–9] under high pressure.

Cobalt oxide (Co_3O_4) is an important magnetic, p-type semiconductor and has been widely used in solid-state

sensors [10], electrochemical devices [11], and heterogeneous catalysts [12]. At ambient conditions, Co_3O_4 is a cubic normal spinel with high-spin (HS) Co^{2+} ions ($S = 3/2$, $e_g^4 t_{2g}^3$) in the tetrahedral sites and low-spin (LS) Co^{3+} ions ($S = 0$, $t_{2g}^6 e_g^0$) in the octahedral sites of the cubic close-packed lattice of oxygen anions. It is well known that Co_3O_4 undergoes a magnetic transition from a high- T paramagnetic state to a low- T long-range-ordered antiferromagnetic (AFM) state at $T_N = 30$ K [13, 14]. The magnetic nature of Co_3O_4 reveals an incommensurate AFM order below T_N [15], with the exchanges of Co^{2+} ions at the 8a site and Co^{3+} ions at the 16d site. The latter study showed that T_N increases with pressure [14], which implies that AFM ordering is accompanied by a negative volume strain. With increasing temperature, there is a cation disorder or charge transfer induced LS–HS transition of the Co^{3+} ion at the 16d site. Previous studies at both high and low temperatures indicated that there is strong coupling among electronic and magnetic properties and their strain conditions. However, no

high-pressure studies have been reported thus far, to the best of our knowledge, addressing structural changes with pressure as well as the associated electronic and magnetic properties. The purpose of this paper is to report our experimental work on the structural, vibrational, and electronic behavior of Co_3O_4 under high pressure using powder XRD, Raman scattering and XANES methods. These studies reveal a structural change associated with a charge transfer process from Co^{2+} to Co^{3+} via hybridization with oxygen atoms under high pressures.

2. Experimental methods

Co_3O_4 powder (US Research Nanomaterials, Inc.) with particle sizes of $\sim 2.5 \mu\text{m}$ was loaded into a $100 \mu\text{m}$ hole of a $35 \mu\text{m}$ thick preindented rhenium gasket. For all measurements, pressure was generated by a symmetric diamond anvil cell (DAC) with diamond culet diameter of $300 \mu\text{m}$ and calibrated by the ruby fluorescence method.

X-ray diffraction: high pressure powder x-ray diffraction measurements were carried out at the 16-IDB beamline of the High Pressure Collaborative Access Team's facility, at the Advanced Photon Source (APS) in Argonne National Laboratory (ANL). Helium was used as a pressure-transmitting medium, and was loaded at room temperature by using a high-pressure gas-loading system [16]. The x-ray beam size was approximately $5 \mu\text{m} \times 7 \mu\text{m}$ at FWHM, the x-ray beam wavelength was 0.3979 \AA . Diffraction patterns were recorded using a Mar CCD with exposure times between 10 and 60 s. The intensity versus 2θ patterns were obtained using the FIT2D software [17]. Rietveld refinements of the XRD patterns were performed using the FULLPROF software package [18]. Equation of state analysis was performed by means of EOSFIT software.

Raman spectroscopy: in our high-pressure Raman measurements, both a 4:1 methanol–ethanol (ME) mixture and helium were used as pressure-transmitting media in two separate experiments, which went up to 35.1 GPa and 20.1 GPa, respectively. We used the micro-Raman spectrometer at GSECARS sector 13 to collect Raman spectra. An argon-ion laser ($\lambda = 514.5 \text{ nm}$, 50 mW) was used as the excitation source and focused to a spot of diameter $4 \mu\text{m}$ at the sample position in a diamond anvil cell. The Raman scattering light was dispersed using a Spec 0.5 m monochromator with a $1800 \text{ grooves mm}^{-1}$ grating, and detected using a liquid nitrogen cooled CCD detector.

X-ray absorption near edge spectroscopy: XANES spectra of the Co K-edge were recorded at the 16-BMD beamline of HP-CAT, with the x-ray beam passing through a beryllium gasket. The x-ray beam size was approximately $7 \mu\text{m} \times 11 \mu\text{m}$. Helium was used as pressure-transmitting medium for pressures up to 24.6 GPa.

3. Results and discussions

3.1. X-ray diffraction

All diffraction patterns measured for pressures up to 42.1 GPa were analyzed by full-profile (Rietveld) refinements. The

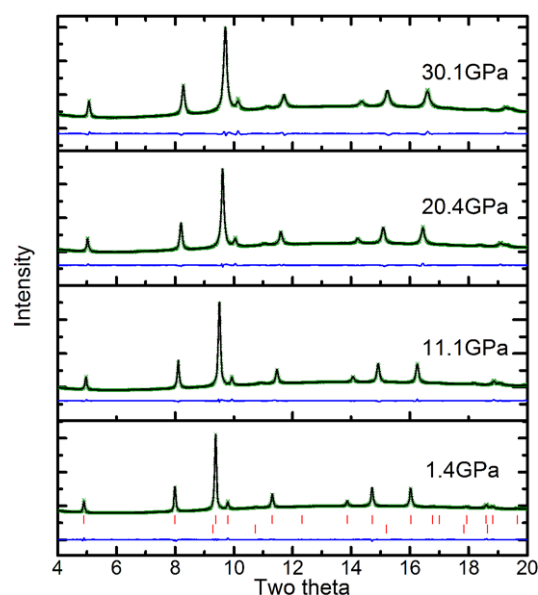


Figure 1. Observed (olive points), calculated (solid black line), and difference (solid blue line) x-ray powder diffraction patterns for Co_3O_4 at selected pressure (indicated). The diffraction patterns are refined assuming an admixture of CoO phase. Red vertical markers indicate Bragg reflections of the two phases (upper: Co_3O_4 ; lower: CoO).

refined parameters include the lattice parameters, the atomic positions of oxygen, isotropic thermal parameters for all atomic sites, a polynomial background, Pseudo-Voigt profile parameters, and an overall intensity scaling factor. For all diffraction patterns, convergence was achieved at residuals (with a subtracted background) $R_{wp} < 2\%$. At pressures above 33.4 GPa, only lattice parameters were extracted from the diffraction patterns. Figure 1 displays the XRD results of the sample in helium medium with the refinement results for the patterns collected at 1.4, 11.1, 21.4, and 31.1 GPa. A small amount of CoO impurity was detected in the diffraction patterns. Two-phase refinements were performed in order to account for the admixture of CoO. Our diffraction results show that the cubic phase of Co_3O_4 remains within the pressure range up to 42.1 GPa.

One refinement result is the oxygen position u , which is generally used as an indicator of cation ordering or disordering within the spinel structure [1, 19–23]. The oxygen position parameters obtained at various pressures are presented in figure 2 (upper panel). The oxygen position u -values decreases linearly with pressure ($u = 0.2632(1) - 0.00009(1)P$, where P is in GPa) below 17.7 GPa and then slightly increase with pressure above 17.7 GPa up to 33.4 GPa. During the pressure releasing process, the oxygen position parameter u -values are smaller than those during the loading process. After pressure releasing to ambient conditions, the oxygen position parameter is much smaller than that before the initiation of compression. It is interesting to compare the results with other spinels. All the normal spinels, such as MgAl_2O_4 [1, 24], ZnAl_2O_4 [25] and ZnGa_2O_4 [26], display a negative pressure dependence of u -values under pressure, which is in qualitative agreement with our results for Co_3O_4

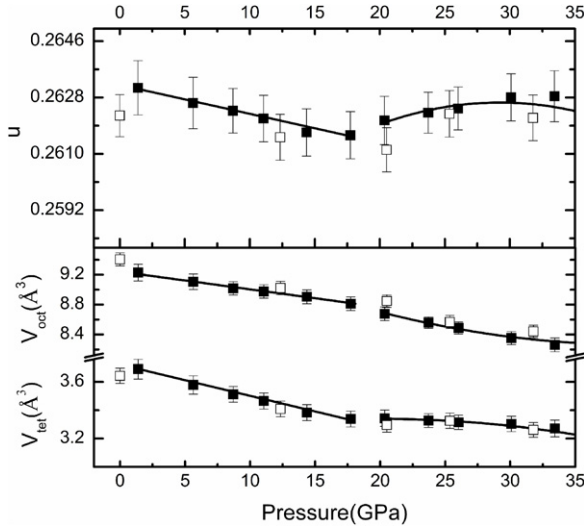


Figure 2. The upper panel gives the pressure evolution of oxygen position parameter u , the lower panel gives the pressure evolution of the polyhedral volume. Solid symbols: loading pressure. Open symbols: unloading pressure. Solid line: linear fit to experiments.

below 17.7 GPa. However, in the inverse spinels, such as Fe_3O_4 [27–30] and $\gamma\text{-Ni}_2\text{SiO}_4$ [31], the u parameter values remain constant or slightly increase with pressure, which shows a similar trend to our results for Co_3O_4 at pressures above 17.7 GPa. The changes in u -values suggest that there may be a structural change for Co_3O_4 from normal spinel to inverse spinel at 17.7 GPa.

The polyhedral volume in a spinel structure can be derived from the lattice parameter a and oxygen position u .

$$V_{\text{tet}} = \frac{64}{3} V \left(u - \frac{1}{8} \right), \quad V_{\text{oct}} = \frac{128}{3} V \left(u - \frac{3}{8} \right) u. \quad (1)$$

The compression effect of polyhedral volumes of the octahedron and the tetrahedron are shown in figure 2 (lower panel). At pressures below 17.7 GPa, the octahedral polyhedron shows a lower compressibility than the tetrahedron. Above 17.7 GPa, the compression behavior is reversed, with the tetrahedron showing a lower compressibility than that of the octahedron. Hazen and Finger [32] demonstrated that the compressibilities of cation-coordinated polyhedra are proportional to the polyhedral volume and inversely proportional to the cation formal valence. Theoretical investigations revealed that a tetrahedron occupied by divalent cations is more compressible than the same occupied by trivalent cations when pressure is applied [22]. If disorder exists between Co^{2+} and Co^{3+} with increasing pressure, before 17.7 GPa, the tetrahedral and octahedral sites are mainly occupied by bivalent and trivalent cations respectively; after 17.7 GPa, this disorder is large enough to change the compressibility of the polyhedrons. The corresponding polyhedral compressibility will change, as we observe in the figure 2 (lower panel).

The bond lengths are given by:

$$\begin{aligned} R_{(\text{Co})-\text{O}} &= a(\sqrt{3}u - 0.125) & \text{and} \\ R_{[\text{Co}]-\text{O}} &= a\sqrt{3u^2 - 2u + 0.375}. \end{aligned} \quad (2)$$

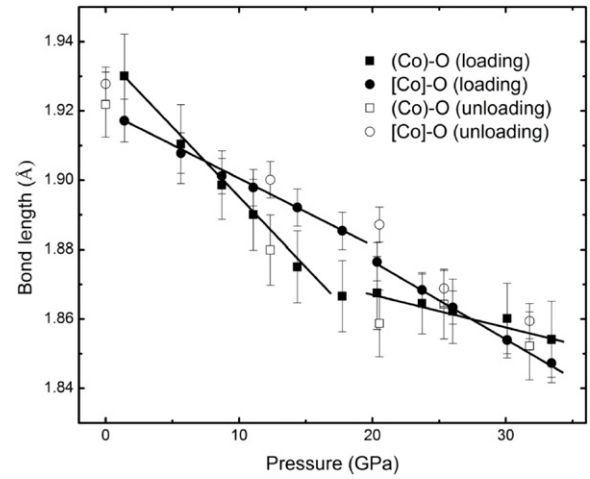


Figure 3. Pressure dependence of the bond lengths on Co_3O_4 . Square: tetrahedral Co–O bond length. Circle: octahedral Co–O bond length. (solid: loading, open: unloading).

As presented in figure 3, the tetrahedral bond length decreases faster than the octahedral bond length at pressures below 17.7 GPa. Above 17.7 GPa, the trend is just reversed, the octahedral bond length decreases faster than the tetrahedral bond length.

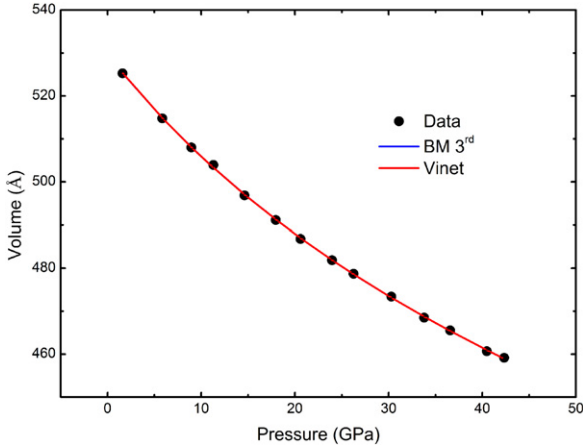
Both the polyhedral compression and the bond length results (figures 2 and 3) suggest an order–disorder transition between the Co^{2+} and Co^{3+} at the tetrahedral and octahedral sites under pressure. The small u -value after pressure release to ambient suggests that the disordered states could be at least partially preserved upon pressure release. Since the cation disorder is generally associated with only small changes in volume [22, 33], the structural transition may leave little or no volume discontinuity with pressure. This is indeed the case, as will be shown below.

The pressure–volume data of Co_3O_4 are shown in figure 4. The volume reduction of Co_3O_4 is $\sim 12.6\%$ in the pressure range of this study. The bulk elastic properties of Co_3O_4 were investigated by the third-order Birch–Murnaghan (BM) equation of state (EOS) [34], and the Vinet EOS [35]. The obtained results are listed in table 1, where P , V , and V_0 denote the pressure, the volume at pressure P , and the volume at ambient pressure, respectively. K_0 and K'_0 are the zero-pressure bulk modulus and its pressure derivative respectively.

The bulk modulus of Co_3O_4 in our study is in close agreement to those reported in previous ab initio studies [36]. The pressure derivative of bulk modulus K'_0 is larger than 4. This result is similar to what was observed in other normal spinels, ZnGa_2O_4 [26], ZnFe_2O_4 [37], ZnAl_2O_4 [25] and MgAl_2O_4 [38]. However, it has been argued that the large value of K'_0 may be explained by a non-hydrostatic effect [39]. To clarify this and the possible normal-to-inverse transition around 17.7 GPa from the discontinuity of u , we used two separate regions in fitting the data (see table 1 for the results). In the low-pressure region, $K'_0(5.1 \pm 1.4)$ is larger than 4. In the high-pressure region, $K'_0(3.9 \pm 1.1)$ is very close to 4 with large values in the bulk modulus. If there

Table 1. Comparison of measured and calculated values of the bulk moduli of Co_3O_4 .

Co_3O_4	EOS	K_0 (GPa)	K'_0	V_0 (\AA^3)
This study	BM	190 ± 5	6.2 ± 0.4	529.60 ± 0.44
	Vinet	189 ± 5	6.3 ± 0.3	529.63 ± 0.43
Theory [36]	M	199	4	549.35
	M	192	4	565.61
$0 \text{ GPa} < P < 17 \text{ GPa}$	BM	199 ± 13	5.1 ± 1.4	529.32 ± 0.65
	BM	203 ± 3	4	528.99 ± 0.37
$17 \text{ GPa} < P < 40 \text{ GPa}$	BM	249 ± 33	3.9 ± 1.1	523.07 ± 3.12
	BM	246 ± 3	4	523.44 ± 0.49

**Figure 4.** Pressure evolution of the volume of Co_3O_4 . The solid blue line represents the third order Birch–Murnaghan EOS fitting result; the red line represents the Vinet EOS fitting result. Errors are within the symbol sizes.

were some non-hydrostatic effect on the bulk modulus, the high-pressure region should give a K'_0 larger than 4. Thus, the non-hydrostatic effect is not the major factor in determining the compression behavior. Both theoretical and experimental results show that the bulk modulus of the inverse spinel is larger than that of the normal spinel, whereas the volume is opposite. From this, we may conclude that there is a gradual transition from normal to inverse spinels before 17 GPa, above which the spinel behaves as an inverse spinel.

The discontinuity of u , the polyhedral volume, the bond length, and the compression behavior with pressure may be a result of a charge transfer between Co^{2+} and Co^{3+} via oxygen. This is due to the fact that charge transfer between Co^{2+} and Co^{3+} requires much lower energy than direct exchange of ions. This charge transfer originates from a different mechanism in the covalence between $(\text{Co}^{2+})\text{-O}$ and $[\text{Co}^{3+}]\text{-O}$ bonds. At ambient conditions, Co_3O_4 presents a covalent component in the primarily ionic bonding character. When the tetrahedral site is occupied by Co^{2+} ($e_g^4 t_{2g}^3$, e_g orbitals are fully occupied and t_{2g} orbitals are half occupied), the e_g orbitals extend toward the edge and the t_{2g} orbitals toward the O^{2-} (though not directly). Thus, the hybridization between the t_{2g} orbitals and orbitals of O^{2-} is stronger than that between the e_g orbitals and the orbitals of O^{2-} . There are three unpaired electrons in the t_{2g} orbitals; when the covalent bonding forms between Co^{2+} and O^{2-} , the unpaired electrons

in the t_{2g} orbitals of Co^{2+} will be paired with the 2p electrons of the oxygen. Thus, the covalent bond is contributed by both Co^{2+} and O^{2-} electrons. On the other hand, at the octahedral site occupied by Co^{3+} ($t_{2g}^6 e_g^0$, t_{2g} orbitals are fully occupied and e_g orbitals are empty), the e_g orbitals extend directly toward the O^{2-} at the vertices and the t_{2g} orbitals extend toward the edges. Thus, the e_g orbitals hybridize more heavily with the orbits of O^{2-} than t_{2g} orbitals. Due to the stronger crystal field energy compared to the spin-paring energy, the t_{2g} orbitals in the Co^{2+} are occupied by three unpaired electrons, whereas the e_g orbitals in the Co^{3+} are unoccupied. When the covalent bond is formed between Co^{3+} and O^{2-} , it is $d^2(e_g)sp^3$ hybridized and all of the bonding electrons will donate to oxygen with the same amounts of spin-up and spin-down electrons [40].

The degree of covalence is strongly dependent upon the bond length and bond angles. From our diffraction data, the bond angle (O-Co-O) in tetrahedral sites remains unchanged at 70.53° under pressure. In octahedral sites, the bond angle change (O-Co-O) with pressure is found to be small and the bond angle is close to 90° . Thus, the degree of covalence is then largely dependent on the bond length. Under pressure, as the bond length decreases, there will be more and more covalent component in both $(\text{Co}^{2+})\text{-O}$ and $[\text{Co}^{3+}]\text{-O}$ bonds. However, the result of this covalent effect is totally different, as discussed before. The Co^{2+} will contribute more unpaired electrons to the covalent bonding, whereas Co^{3+} will accept more paired electrons from oxygen. It thus appears that there is charge transfer from Co^{2+} to Co^{3+} , and this probably cause the spin moment in Co^{2+} to decrease and no spin moment change in Co^{3+} . This view of covalence-induced spin moment is consistent with the observation of a very low spin moment in Co_3S_4 [41].

3.2. XANES results

Cobalt K-edge XANES spectra collected at high pressures are shown in figure 5. The Co K absorption edge spectrum comprises five features contributed by Co^{2+} and Co^{3+} : two pre-edge ($1s\text{-}3d$), two shoulders ($1s\text{-}4s$), and one edge crest ($1s\text{-}4p$) [42]. The pre-edge peak intensity is closely related to the number of 3d electrons, symmetry, and coordination number. The pre-edges from the tetrahedral Co^{2+} are stronger than the octahedral Co^{3+} , due to the tetrahedral ligand field allowing dipole transition, while in the octahedral symmetry,

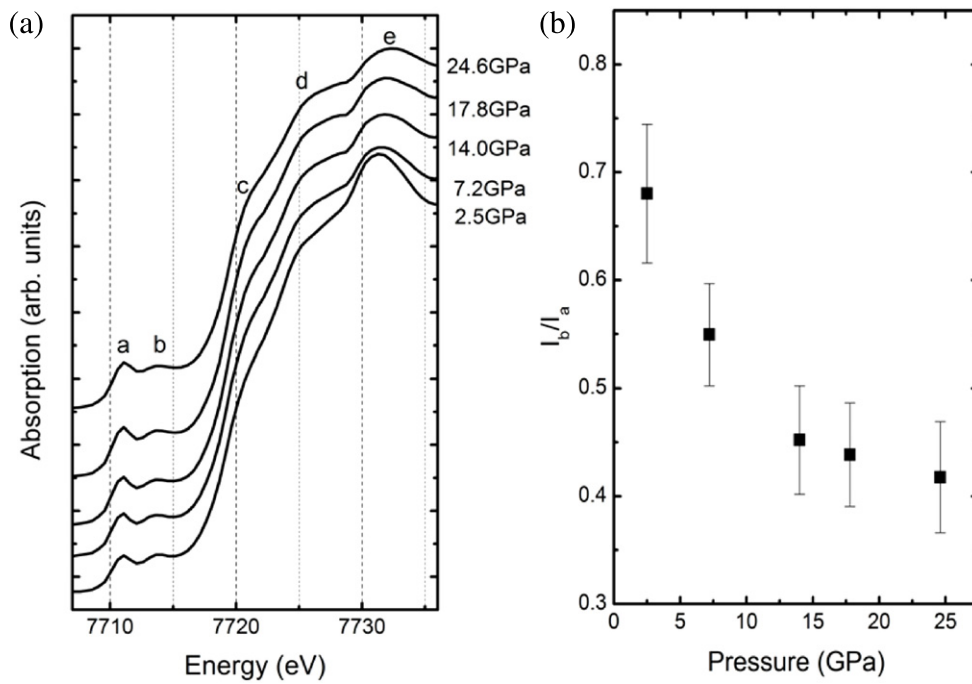


Figure 5. Normalized Co K-edge XANES spectra of Co₃O₄ at selected pressure (left panel, a). Right panel (b) shows the relative integrated peak intensity ratio I_b/I_a changing with pressure.

only weaker quadrupole transition is allowed. Another feature is that the pre-edge from the octahedral site is usually broader than the pre-edge from the tetrahedral site. So the sharper and stronger pre-edge peak *a* (figure 5(a)) located at lower energy position is from the tetrahedral divalent cobalt, and the weaker and broader pre-edge peak *b* at higher energy position is from the octahedral trivalent cobalt. We fitted the pre-edge range using a background and two Gaussian functions to get the integrated intensities of *a* and *b*. Upon compression up to 17 GPa, the relative intensity of I_b/I_a decreases with increasing pressure (figure 5(b)). Within this pressure range, there is no change in the symmetry and coordination number of both sites. Thus, the intensity change can be interpreted as due to the change in the number of 3d electrons or the hybridization of cobalt 3d and oxygen 2p electrons, i.e. the oxidation state. In other words, the relative intensity change in the pre-edge suggests that the changes in the unoccupied Co 3d density of states are the reason for this behavior, implying a charge transfer from the T_d site to the O_h site. The results from our XANES study thus further support the charge transfer process obtained from our XRD data.

3.3. Raman spectroscopy

For Co₃O₄ in the normal spinel structure (Co)[Co]₂O₄ (space group $Fd\bar{3}m$), there are five Raman-active phonon modes $A_{1g} + E_g + 3F_{2g}$ [43]. As shown in figure 6, the Raman data at 2.4 GPa are consistent with those measured at ambient conditions, with five modes observed at 196.7 cm⁻¹ $F_{2g}(1)$, 484.1 cm⁻¹ E_g , 523.1 cm⁻¹ $F_{2g}(2)$, 621.5 cm⁻¹ $F_{2g}(3)$, 693.4 cm⁻¹ A_{1g} . The A_{1g} mode is generally assigned to the symmetric stretching of the Co–O bond in tetrahedral sites,

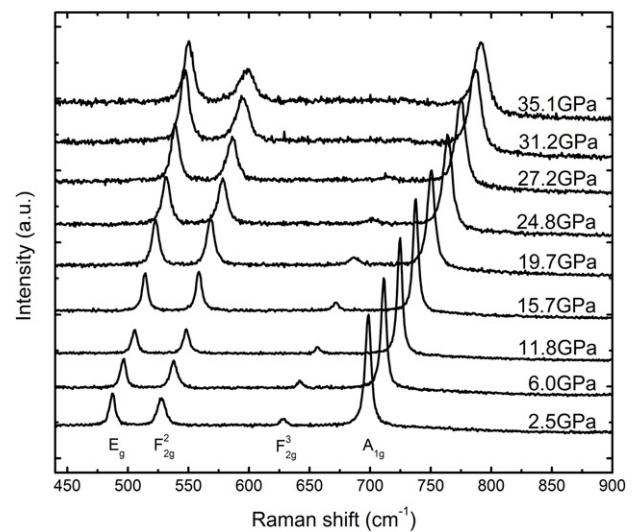


Figure 6. The pressure evolution of Raman spectra at selected pressure for Co₃O₄.

and is often referred to as the tetrahedral breathing mode (TBM).

Figure 6 shows the Raman spectra of Co₃O₄ at different pressures up to 35.1 GPa using ME as pressure-transmitting medium. At first, the Raman bands broaden and shift to higher energies with increasing pressure. The $F_{2g}(1)$ and $F_{2g}(3)$ modes cannot be observed at pressures higher than 15 GPa and 20 GPa, respectively. It is well known that the Grüneisen parameter plays a crucial role in understanding the thermodynamic and thermoelastic behavior of solids. Figure 7 shows the pressure dependence of Raman modes. Using the

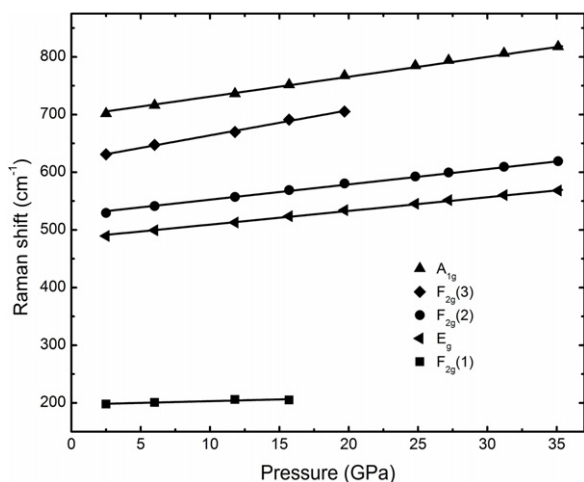


Figure 7. Pressure dependence of Raman mode frequencies. Straight line show the fits to linear function.

Table 2. Ambient-pressure Raman frequencies ω_0 , their pressure dependences $d\omega/dP$, and mode Grüneisen parameter γ of Co_3O_4 .

Modes	ω_0 (cm ⁻¹)	$d\omega/dP$ (cm ⁻¹ GPa ⁻¹)	Grüneisen parameter (γ)
F _{2g} (1)	196.9	0.6	0.57
E _g	485.4	2.4	0.92
F _{2g} (2)	525.9	2.6	0.92
F _{2g} (3)	620.4	4.4	1.32
A _{1g}	696.8	3.4	0.91

definition of the zero-pressure mode Grüneisen parameter γ_0

$$\gamma_0 = - \left(\frac{d \ln \omega}{d \ln V} \right)_{P=0} = \frac{B_0}{\omega_0} \left(\frac{d\omega}{dP} \right)_{P=0}$$

where ω and ω_0 are the Raman frequencies under pressure and at ambient conditions, B_0 the bulk modulus. Combined with our XRD experimental value of the bulk modulus $B_0 = 187$ GPa, the obtained ambient-pressure Raman frequencies ω_0 , their pressure derivatives $d\omega/dP$ and the mode Grüneisen parameters γ_0 are shown in the table 2. There was no discontinuity during this charge transfer process.

Summary

The structural, vibrational, and electronic properties of the cubic spinel of Co_3O_4 have been studied under pressure by x-ray diffraction, Raman spectroscopy, and XANES. The cubic phase of Co_3O_4 is stable in the pressure range of this study. The analyses of structural refinements show the discontinuities of oxygen position, bond length, and polyhedral volume at high pressure, which can be explained by a charge transfer process via hybridization between cobalt and oxygen. The change marks a structural transition from the normal-type spinel to a partially inverse-type spinel at 17.7 GPa. The result from XRD is supported by the changes in the unoccupied Co 3d density of state, which was evidenced in XANES measurements under high pressures. From the Raman measurements, we obtained the Grüneisen parameters, and no discontinuity was observed.

Acknowledgments

We thank Y M Xiao and Y Ding for helpful discussions. We acknowledge support from the DOE Cooperative Agreement No. DE-FC08-01NV14049 with the University of Nevada, Las Vegas. This work was performed at HPCAT (Sector 16), Advanced Photon Source (APS), Argonne National Laboratory (ANL). HPCAT is supported by CIW, CDAC, UNLV, and LLNL through funding from DOE-NNSA, DOE-BES, NSF, and W M Keck Foundation. Use of the Advanced Photo Source is supported by the DOE Office of Science, Office of Basic Energy Sciences, under Contract No. DE-AC02-06CH11357. We thank GSECARS, at the APS, ANL for the use of their gas-loading and Raman setup.

References

- [1] Wittlinger J, Werner S and Schulz H 1998 Pressure-induced order-disorder phase transition of spinel single crystals *Acta Crystallogr. B* **54** 714–21
- [2] Meducin F, Redfern S A T, Le Godec Y, Stone H J, Tucker M G, Dove M T and Marshall W G 2004 Study of cation order-disorder in MgAl_2O_4 spinel by *in situ* neutron diffraction up 1600 K and 3.2 GPa *Am. Mineral.* **89** 981–6
- [3] Chen Q Y, Meng C M, Lu T C, Xu M, Qi J Q and Tan J J 2010 Shock-induced cation disorder in magnesium aluminate spinel *J. Appl. Phys.* **108** 113522
- [4] Takeda K *et al* 2005 Pressure-induced charge ordering of LiV_2O_4 *Physica B* **359** 1312–4
- [5] Okada H, Koyama K, Hedo M, Uwatoko Y and Watanabe K 2008 Pressure-induced metal-insulator transition in spinel compound CuV_2S_4 *Physica B* **403** 1612–3
- [6] Furubayashi T, Kosaka T, Tang J, Matsumoto T, Kato Y and Nagata S 1997 Pressure induced metal-insulator transition of selenospinel CuIr_2Se_4 *J. Phys. Soc. Japan* **66** 1563–4
- [7] Fava F F, Baraille I, Lichanot A, Larrieu C and Dovesi R 1997 On the structural, electronic and magnetic properties of MnCr_2O_4 spinel *J. Phys.: Condens. Matter* **9** 10715–24
- [8] Choi H, Shim J and Min B 2006 Electronic structures and magnetic properties of spinel ZnMn_2O_4 under high pressure *Phys. Rev. B* **74** 172103
- [9] Ding Y, Haskel D, Ovchinnikov S, Tseng Y-C, Orlov Y, Lang J and Mao H-K 2008 Novel pressure-induced magnetic transition in magnetite (Fe_3O_4) *Phys. Rev. Lett.* **100** 045508
- [10] Ando M, Kobayashi T, Iijima S and Haruta M 1997 Optical recognition of CO and H_2 by use of gas-sensitive Au- Co_3O_4 composite films *J. Mater. Chem.* **7** 1779–83
- [11] Svegl F, Orel B, Hutchins M G and Kalcher K 1996 Structural and spectroelectrochemical investigations of sol-gel derived electrochromic spinel Co_3O_4 films *J. Electrochem. Soc.* **143** 1532–9
- [12] Yan L, Zhang X, Ren T, Zhang H, Wang X and Suo J 2002 Superior performance of nano-Au supported over Co_3O_4 catalyst in direct N_2O decomposition *Chem. Commun.* **860**–1
- [13] Roth W L 1964 The magnetic structure of Co_3O_4 *J. Phys. Chem. Solids* **25** 1–10
- [14] Ikedo Y, Sugiyama J, Nozaki H, Mukai K, Itahara H, Russo P L, Andreica D and Amato A 2009 High pressure mu SR study on cobalt oxide spinel *Physica B* **404** 652–5
- [15] Ikedo Y, Sugiyama J, Nozaki H, Itahara H, Brewer J H, Ansaldo E J, Morris G D, Andreica D and Amato A 2007 Spatial inhomogeneity of magnetic moments in the cobalt oxide spinel Co_3O_4 *Phys. Rev. B* **75** 054424

- [16] Rivers M, Prakapenka V B, Kubo A, Pullins C, Holl C M and Jacobsen S D 2008 The COMPRES/GSECARS gas-loading system for diamond anvil cells at the advanced photon source *High Press. Res.* **28** 273–92
- [17] Hammersley A P 1997 FiT2D: an introduction and overview *ESRF Internal Report*
- [18] Rodríguez-Carvajal J 1993 Recent advances in magnetic structure determination by neutron powder diffraction *Physica B* **192** 55–69
- [19] O'Neill H S C and Navrotsky A 1983 Simple spinels—crystallographic parameters, cation radii, lattice energies, and cation distribution *Am. Mineral.* **68** 181–94
- [20] Redfern S A T, Harrison R J, O'Neill H S C and Wood D R R 1999 Thermodynamics and kinetics of cation ordering in MgAl_2O_4 spinel up to 1600 °C from *in situ* neutron diffraction *Am. Mineral.* **84** 299–310
- [21] O'Neill H S C, James M, Dollase W A and Redfern S A T 2005 Temperature dependence of the cation distribution in CuAl_2O_4 spinel *Eur. J. Mineral.* **17** 581–6
- [22] Recio J M, Franco R, Martín Pendás A, Blanco M A, Pueyo L and Pandey R 2001 Theoretical explanation of the uniform compressibility behavior observed in oxide spinels *Phys. Rev. B* **63** 184101
- [23] Wei S-H and Zhang S B 2001 First-principles study of cation distribution in eighteen closed-shell $A^{II}B_2^{III}O_4$ and $A^{IV}B_2^{II}O_4$ spinel oxides *Phys. Rev. B* **63** 045112
- [24] Finger L W, Hazen R M and Hofmeister A M 1986 High-pressure crystal chemistry of spinel (MgAl_2O_4) and magnetite (Fe_3O_4): comparisons with silicate spinels *Phys. Chem. Miner.* **13** 215–20
- [25] Levy D, Pavese A, Sani A and Pischedda V 2001 Structure and compressibility of synthetic ZnAl_2O_4 (gahnite) under high-pressure conditions, from synchrotron x-ray powder diffraction *Phys. Chem. Miner.* **28** 612–8
- [26] Errandonea D, Kumar R S, Manjón F J, Ursaki V V and Rusu E V 2009 Post-spinel transformations and equation of state in ZnGa_2O_4 : determination at high pressure by *in situ* x-ray diffraction *Phys. Rev. B* **79** 024103
- [27] Gatta G D, Kantor I, Ballaran T B, Dubrovinsky L and McCammon C 2007 Effect of non-hydrostatic conditions on the elastic behaviour of magnetite: an *in situ* single-crystal x-ray diffraction study *Phys. Chem. Miner.* **34** 627–35
- [28] Glazyrin K, McCammon C, Dubrovinsky L, Merlini M, Schollenbruch K, Woodland A and Hanfland M 2012 Effect of high pressure on the crystal structure and electronic properties of magnetite below 25 GPa *Am. Mineral.* **97** 128–33
- [29] Rozenberg G, Amiel Y, Xu W, Pasternak M, Jeanloz R, Hanfland M and Taylor R 2007 Structural characterization of temperature- and pressure-induced inverse \leftrightarrow normal spinel transformation in magnetite *Phys. Rev. B* **75** 020102
- [30] Haavik C, Stølen S, Fjellvåg H, Hanfland M and Häusermann D 2000 Equation of state of magnetite and its high-pressure modification: thermodynamics of the Fe–O system at high pressure *Am. Mineral.* **85** 514–23
- [31] Finger L W, Hazen R M and Yagi T 1979 Crystal structures and electron densities of nickel and iron silicate spinels at elevated temperature or pressure *Am. Mineral.* **64** 1002–9
- [32] Hazen R M and Finger L W 1979 Bulk modulus–volume relationship for cation–anion polyhedra *J. Geophys. Res.* **84** 6723–8
- [33] Seko A, Yuge K, Oba F, Kuwabara A and Tanaka I 2006 Prediction of ground-state structures and order–disorder phase transitions in II–III spinel oxides: a combined cluster-expansion method and first-principles study *Phys. Rev. B* **73** 184117
- [34] Birch F 1947 Finite elastic strain of cubic crystals *Phys. Rev.* **71** 809–24
- [35] Vinet P, Ferrante J, Smith J R and Rose J H 1986 A universal equation of state for solids *J. Phys. C: Solid State Phys.* **19** L467
- [36] Chen J, Wu X and Selloni A 2011 Electronic structure and bonding properties of cobalt oxide in the spinel structure *Phys. Rev. B* **83** 245204
- [37] Levy D, Pavese A and Hanfland M 2000 Phase transition of synthetic zinc ferrite spinel (ZnFe_2O_4) at high pressure, from synchrotron x-ray powder diffraction *Phys. Chem. Miner.* **27** 638–44
- [38] Levy D, Pavese A and Hanfland M 2003 Synthetic MgAl_2O_4 (spinel) at high-pressure conditions (0.0001–30 GPa): a synchrotron x-ray powder diffraction study *Am. Mineral.* **88** 93–8
- [39] Greenberg E, Rozenberg G K, Xu W, Arielly R, Pasternak M P, Melchior A, Garbarino G and Dubrovinsky L S 2009 On the compressibility of ferrite spinels: a high-pressure x-ray diffraction study of MFe_2O_4 ($M = \text{Mg}, \text{Co}, \text{Zn}$) *High Press. Res.* **29** 764–79
- [40] Owen J and Thornley J H M 1966 Covalent bonding and magnetic properties of transition metal ions *Rep. Prog. Phys.* **29** 675
- [41] Miyazaki S, Shirai M and Suzuki N 1998 Electronic band structure of antiferromagnetic spinel Co_3S_4 *J. Magn. Magn. Mater.* **177–181** 1367–8
- [42] Jiang T and Ellis D E 1996 X-ray absorption near edge structures in cobalt oxides *J. Mater. Res.* **11** 2242–56
- [43] Hadjiev V G, Iliev M N and Vergilov I V 1988 The Raman spectra of Co_3O_4 *J. Phys. C: Solid State Phys.* **21** L199